AEGC2019 Data to Discovery
Australasian Exploration Geoscience Conference
2-5 September 2019 • Perth, Western Australia
Incorporating the AIG, ASEG, PESA, and WABS

3D inversion of electromagnetic logging-while-drilling data

David Marchant*
Computational Geosciences Inc.
Vancouver, BC, Canada
dave@compgeoinc.com

Nigel Clegg
Halliburton
Great Yarmouth, UK
nigel.clegg@halliburton.com

Luke Rawsthorne
Aker BP
Stavanger Norway
luke.rawsthorne@akerbp.com

Jari Kunnas
Halliburton
Stavanger, Norway
jari.kunnas@halliburton.com

SUMMARY

Electromagnetic logging while drilling is commonly used to infer information about the electrical properties around the wellbore and to aid in geosteering. Data from modern tools, which combine multiple transmitter and receiver orientations and offsets, can be difficult to manually interpret in all but the simplest of environments. Inversion is required to optimally extract and use the information from this data. Although low dimensional inversions can provide useful information in certain environments, full, 3D solutions are required to extract the maximum possible amount of information from the data.

In this work, we present the first fully 3D inversion of electromagnetic logging-while-drilling data. Moreover, we demonstrate that using semi-structured meshing and mesh decoupling, along with advanced data integration techniques, enables the inversions to be performed in real time.

Key words: inversion, electromagnetic, borehole geophysics, three-dimensional

INTRODUCTION

Electromagnetic logging-while-drilling (LWD) data uses an array of multiple transmitter and receiver coils placed behind the drill bit to collect information about the electrical properties of the drilling environment (Sviridov et al., 2014; Dupuis and Denichou, 2015; Wu et al., 2018). This information is routinely inverted in one or two dimensions to recover a picture of the resistivity distribution around the borehole and to simplify the interpretation process (Abubakar et al., 2008, Bakr et al., 2017, Thiel and Omeragic, 2018). These lower-dimensional tools can provide excellent results when changes in the earth's resistivity are also limited to one or two dimensions. However, these approaches can fail significantly when applied in the presence of 3D structures.

Modeling and inverting the data that are generated by these tools presents several challenges. First, one must be able to model the data, that is, solve Maxwell's equations in a 3D inhomogeneous medium to simulate the response and sensitivities of the tool. Second, the data must be inverted in such a way as to produce a geologically meaningful model. If these inversions are performed with the goal of guiding the drilling process, the inversion results must be computed quickly. Ideally, the inversions should complete at the same rate at which new data are being acquired by the system. Finally, to make these completion times possible, new data must be injected into the inversion in an intelligent fashion to optimally use the previously completed computations.

In this work, we describe our approach to overcoming each of these challenges. The methodology is then applied to a simple synthetic example to demonstrate its viability. Finally, a case study for tri-lateral well placement in a mature reservoir in the Norwegian Continental shelf is presented.

METHODOLOGY

In this section, we discuss the methods applied in the solution of the forward and inverse problems.

Forward Modeling Methodology

The LWD and induction logging problem involves imaging a narrow and long volume within the earth. An efficient discretization uses small cells in the vicinity of the borehole and larger cells further away. We use octree meshes that have been successfully applied for other adaptive electromagnetic inversions (Haber and Schwarzbach, 2014). Using this style of mesh provides several benefits over fully unstructured meshes. In particular, unlike a fully unstructured mesh, the interpolation of models and fields from one octree to another is a trivial operation.

The quasi-static approximation of Maxwell's equations is

$$\nabla \times E_{ij} + i\omega_j B_{jk} = 0$$
$$\nabla \times \mu^{-1} B_{jk} + \sigma E_{jk} = s_k$$

where E and B are the electric field and magnetic flux respectively, $\mu = \mu_0$ is the magnetic permeability and is assumed to be constant, ω is the angular frequency, σ is the conductivity, and s is the source. The electrical resistivity is the inverse of conductivity, $\rho = \frac{1}{\sigma}$. Boundary conditions are applied to the tangential components of the electric conductivity or its curl. The indices j = 1, . . ., n_w and k = 1, . . ., n_s imply that we have n_w frequencies and n_s sources to describe the complete forward problem. In the forward problem, we assume that σ is known and aim to solve for E and B for all sources and frequencies. A typical survey can contain tens of frequencies and (depending on borehole length) a few hundred or even thousands of source locations. Considering all frequencies and sources, this can amount to having to solve hundreds, if not thousands, of discrete

Maxwell's equations to simulate the complete data set. Using one mesh that contains the complete borehole would be too computationally expensive to be practical. Thus, we decouple the forward meshes from the inverse mesh and one another, and discretize every frequency and location on its own mesh. Figure 1 provides an example of such a mesh. In this example, more than 500,000 cells describe the full-length of the borehole, but only 30,000 cells for the discretization of the forward problem with a single transmit location.

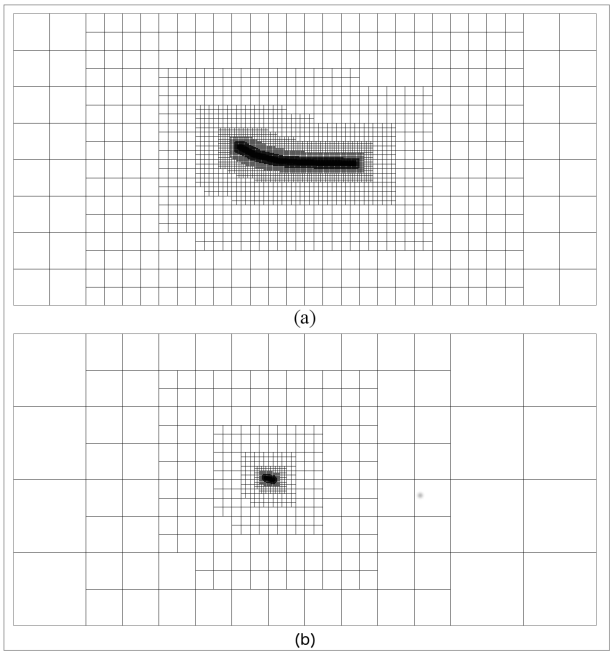

Figure 1. Cross-section of the octree mesh discretizes the conductivity around a borehole (a) The global mesh holds the entire inversion model (b). A local mesh is refined only in the area of a single measurement location.

The discrete analogue of Maxwell's equations on the staggered forward meshes is

$$\left(C_{jk}^{T} M_{jk}(\mu^{-1}) C_{jk} + i\omega_j M_{jk}(P_k\sigma)\right) u_{jk} = -i\omega_j s_k$$

Here, C is the discretization of the curl operator, $M_{jk}(\mu^{-1})$ is a face mass matrix for the permeability, $M_{jk}(P_k\sigma)$ is an edge mass matrix for the conductivity, and u is the discrete electric field. The matrix P_k projects the fine scale conductivity onto the coarse forward mesh, and the j and j indices imply that each mesh has its own operators.

Because the individual linear systems are independent of one another, they can be solved using a direct solver in parallel, which, for the smaller meshes requires only a few seconds (depending on the computational architecture) on individual processors. Using modest computational hardware, with 40 cores, we can solve the complete forward problem for all sources and frequencies in a few seconds. This is crucial for obtaining real-time solutions for LWD data.

Inverse Modeling Methodology

To perform the 3D inversion, we minimize a combination of data misfits and regularization

$$\min_m \sum_{jk} \left\| Q_{jk} u_{jk}(m) - d_{jk} \right\|_{W_{ij}}^2 + \alpha R(m)$$

Here, $m = \log(\sigma)$ is the log-conductivity, Q_{jk} is a matrix that projects the curl of E to the measuring location and orientation, d_{jk} is the data that is measured for the jth frequency and kth source, W_{ij} is the inverse covariance matrix for the data, and $R(m)$ is the regularization with a trade-off parameter α. The regularization is designed to encourage smooth results close to a pre-defined reference model. It is expressed as

$$R(m) = \alpha_s \left\| m - m_{ref} \right\|^2 + \left\| S(\theta,\phi) G(m - m_{ref}) \right\|^2$$

Here, G is a finite difference matrix that represents the gradient, m_{ref} is a reference model that contains the best guess for the conductivity, and $S(\theta,\varphi)$ is a rotation matrix. If the media under consideration is layered and the layers coincide with the direction of the mesh, then $S = I$. Otherwise, if we have *a priori* knowledge of the media's orientation, then we choose S such that smoothness is used in the direction of the layers.

The optimization problem is solved using a Gauss-Newton method to take advantage of matrix-vector products; sensitivities are thus never computed explicitly. Because direct methods are used for the solution of the forward problem, the factorizations of the forward matrices can be stored, and the sensitivity calculation is completed in seconds using parallel computations. Thus, a single Gauss-Newton step requires a few seconds, and the 3D inversion is complete in a matter of minutes.

Real-Time Inversion

One of the unique attributes of the LWD imaging problem is that data are meant to be inverted in real time, beginning with very little data. The model is slowly built up as new data become available. Continually updating a model as data are added is a classical control and data-assimilation problem. Here, we use an extension of non-linear Kalman filtering, which is a common approach from the weather-prediction field. Assume we have data for p sources and frequencies and have solved the optimization problem to obtain a model m_p. Consider now adding new data and recovering the next model m_{p+1}. An efficient way to consider the previously collected data is to modify the regularization, as discussed in Fohring and Haber (2016), so that

$$R(m) = \alpha_s \left\| m - m_p \right\|^2 + \left\| S(\theta,\phi,m_p) G(m - m_p) \right\|^2$$

The reference model in the regularization is replaced with the model obtained in the last inversion. Note that we are also able to add new orientation information based on previous models.

SYNTHETIC EXAMPLE

In this section, the technique is demonstrated on a synthetic example of a simple 3D reservoir model that includes varying dips, strikes, faults, and folding, and includes resistivities ranging from 1 to 50 Ωm. Figure 2 shows the true model, with the simulated well path shown by the dashed white line. The layers are flat-lying in the north-south direction at x = 1600 m, but the dip gradually increases to 30° to the north (into the page) at x = 1800 m and then slowly changes to 30° to the south (out of the page) at x = 2200 m.

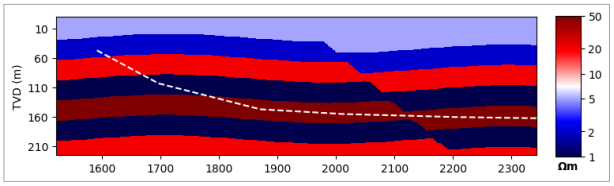

Figure 2. Vertical cross-section of the synthetic resistivity model. The simulated well path is shown by the dashed white line.

LWD data were simulated for three transmitter-receiver spacings (25, 50, and 100 ft) at five frequencies ranging from 1 to 16 kHz, with logging depths approximately every 3 m (approximately 10 ft) along the deviated well trajectory. Gaussian noise with a standard deviation of 5% of the channels value plus 10^{-8} V/A was added to the simulated response. During inversion, data from 15 logging depths were inverted at a time. The global mesh was discretized with a total of 576,550 cells. The local modeling meshes were discretized as 0.5 m cubes in the proximity of the transmitters and receivers, and the cell size increased with distance from the wellbore. The global model was initiated with a homogeneous, 10-Ωm whole-space. No additional a priori information was included in the model objective function.

Figure 3 presents slices taken from the inversion result parallel to the direction of drilling at three different stages of logging. In this case, visualization of the inversion model is clipped to 50 ft radius around the wellbore. The evolution of the inversion model can be easily observed, with recovery of the formation resistivity and structure improving as additional data are acquired. Figure 4 shows slices taken from the resulting model at the same three points perpendicular to the direction of drilling. The dashed black lines indicate the true location and dip of the layer boundaries at these three locations. The inversion provides excellent recovery of the true model.

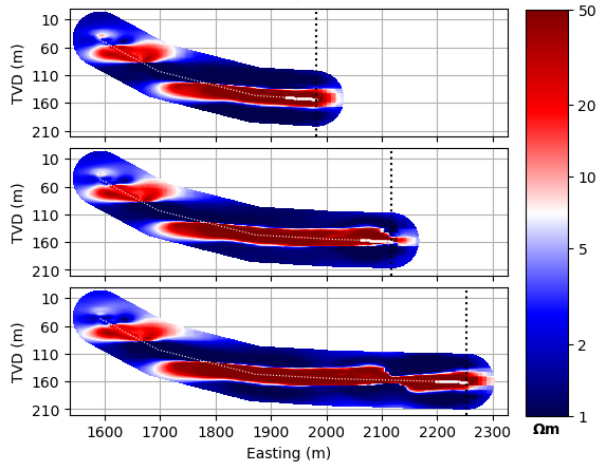

Figure 3. Slices of the inversion result taken at three points during the inversion. The location of the leading transmitter is shown with the dotted black line.

In terms of computational performance, the inversion was run on a single cluster node with 24 cores and 512 GB of memory. The inversion required 13.9 hours to run, with an average inversion runtime of 226 seconds per logging depth. Even with the increased model complexity, this is still well within the expectation of 300 seconds (5 minutes) for additional data of this type of sensor.

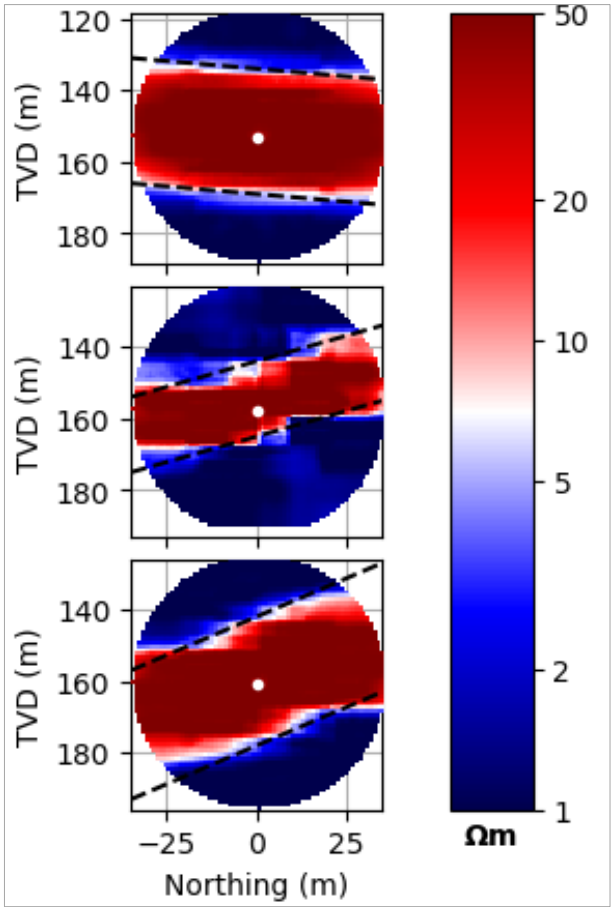

Figure 4. Slices of the inversion result taken perpendicular to the direction of drilling at the same three locations shown in Figure 3. The dashed black lines show the true location and dip of the layer boundaries.

CASE STUDY

The ultra-deep electromagnetic LWD data for three branches of a multi-lateral well drilled on the Norwegian Continental Shelf were inverted using the 3D inversion process. Real-time 1D inversions were analyzed to assist in the well placement operation; however, it was clear that, although this was sufficient to assist in well placement in terms of corrections to inclination, there was the potential for significant changes in the geology to the sides of the wellbore that could not be assessed using the 1D inversion alone. In addition, where a 1D inversion is used to represent a 3D geological structure, the changes in resistivity to the sides of the wellbore can affect the 1D inversion itself, resulting in a distortion of the represented geology.

The target for these wells was a complex turbidite reservoir consisting of heterolithic sands resulting from the depositional environment and the potential for complex fluid contacts. In this subsurface environment, the potential existed for significant changes in resistivity to the sides of the borehole that would not be accounted for in a 1D inversion.

Ultra-deep azimuthal resistivity images available from the tool run in this reservoir enabled changes in resistivity a significant distance to the sides of the borehole to be assessed and

changes in resistivity tracked (Clegg et al., 2018). This enabled a simplified assessment of the distribution of fluids and formations to the sides of the borehole (Figure 5). Although this is a simplified picture, it enables an independent assessment of the 3D inversion results.

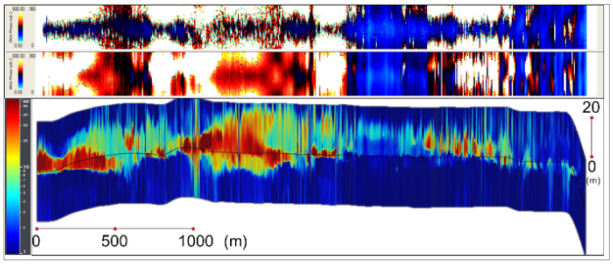

Figure 5. 2 and 8 kHz azimuthal resistivity images and 1D inversion canvas for the main bore of the tri-lateral well.

If changes in resistivity were simply above and below the tool, as represented in the 1D inversion, then the azimuthal resistivity images would be symmetrical. However, it is clear that many of the changes in resistivity occur to the sides of the well, as demonstrated by the non-symmetrical nature of the images.

An inversion perpendicular to the well would capture some of these lateral changes, but is still a simplification of what is a complex 3D structure. A 3D inversion is required to accurately represent this complex geology (Figure 6).

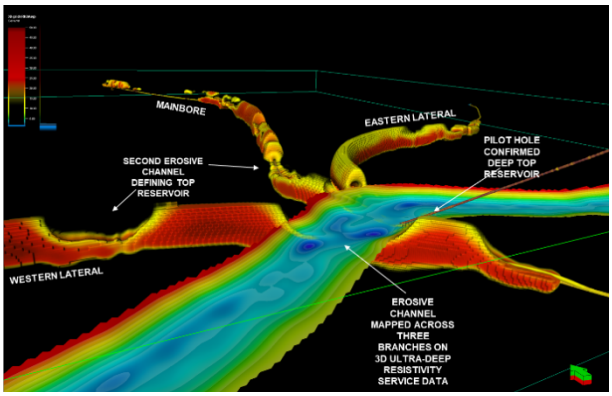

Figure 6. 3D inversion results for all three laterals. The channel that has resulted in significant erosion of the reservoir has been interpreted from the ultra-deep electromagnetic data.

The complex nature of the turbidite deposits is clear from the 1D inversions; however, it is the 3D results that provide a deeper understanding of the reservoir. In the initial parts of the three lateral wells, the data show that, in many places, the resistivity is offset to the sides of the well path (Figure 7). This is also evident in the azimuthal resistivity images.

In the latter parts of the well, the 3D inversion results reveal a complex reservoir morphology, suggesting channel or possibly injectite structures (Figure 8).

The 1D inversion and azimuthal resistivity images show a simplification of what is a very complex geology. The 3D inversion results provide a much clearer picture.

In real-time well placement operations, the 3D inversion will enable improved geosteering that takes into account both lateral changes and changes above and below the wellbore.

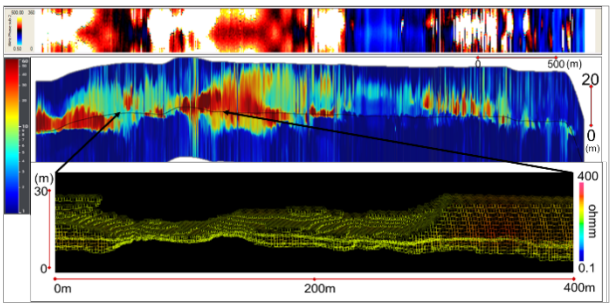

Figure 7. Top: azimuthal resistivity image, showing high resistivity to the left of the well; middle: 1D inversion canvas; and bottom: 3D inversion results, which also show high resistivity distributed to the left of the wellbore.

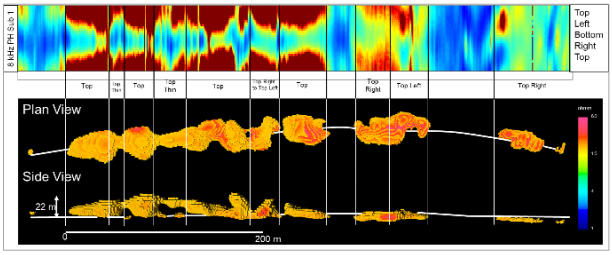

Figure 8. Channel-like structures toward the toe of the main bore. Top: 8 kHz azimuthal resistivity image; bottom: top-down and side views of the 3D inversion results.

CONCLUSIONS

In this work, we have developed a method for real-time inversion of LWD data that uses a mesh decoupling approach to reduce the cost of the forward and inverse computations. In addition, we have used new data assimilation algorithms to aid in further computational reductions as new data are recorded. A simple experiment shows that such data can be successfully inverted in real time, even on modest computational hardware.

ACKNOWLEDGEMENTS

The authors thank AkerBP for supporting the ultra-deep resistivity 3D inversion trials, and acknowledge partners ConocoPhillips and Lundin Norway for permission to publish. The authors also thank Halliburton Energy Services Inc. and Computational Geosciences Inc. for permission to publish.

REFERENCES

Abubakar, A., Habashy, T.M., Druskin, V.L., Knizhnerman, L., and Alumbaugh, D., 2008, 2.5D forward and inverse modeling for interpreting low-frequency electromagnetic measurements: Geophysics, 75 (4), F165-F177.

Bakr, S., Pardo, D., and Torres-Verdin, C., 2017, Fast inversion of logging-while-drilling resistivity measurements acquired in multiple wells: Geophysics, 82, E111-E120.

Clegg, N., Djefel, B., Kunnas, J., and Kuld, I., 2018, Identification and projected interception of oblique faults up to 85 ft away using ultra-deep azimuthal resistivity and geosignals: A case history from the Norwegian Continental Shelf. Presented at Abu Dhabi International Petroleum

Exhibition and Conference, Abu Dhabi, UAE, 12-15 November. SPE-192854-MS. https://doi.org/10.2118/192854-MS.

Dupuis, C. and Denichou, J.M., 2015, Automatic inversion of deep-directional-resistivity measurements for well placement and reservoir description: The Leading Edge, 34 (5), 504-512.

Fohring, J. and Haber, E., 2016, Adaptive a-optimal experimental design for linear dynamical systems: SIAM/ASA Journal of Uncertainty Quantification, 4 (X), 1138-1159.

Haber, E. and Schwazbach, C., 2014, Parallel inversion of large-scale airborne time-domain electromagnetic data with multiple OcTree meshes: Inverse Problems, 30 (5).

Sviridov, M.V., Mosin, A., Antonov, Y., Nikitenko, M., Martakov, S., and Rabinovich, M., 2014, New software for processing LWD extra deep resistivity and azimuthal resistivity data: SPE Reservoir Evaluation and Engineering, 17 (2). SPE-160257-PA. https://doi.org/10.2118/160257-PA.

Thiel, M. and Omeragic, D., 2018, Azimuthal imaging using deep-directional resistivity measurements reveals 3D reservoir structure: Presented at SPWLA 59th Annual Logging Symposium, London, UK, 2-6 June. SPWLA-2018-S..

Wu, H.-H., Golla, C., Parker, T., et al., 2018, A new ultra-deep azimuthal electromagnetic LWD sensor for reservoir insight. Presented at the SPWLA 59th Annual Logging Symposium, London, UK, 2-6 June. SPWLA-2018-X.